Helium-dislocation interaction in aluminium

2001 J. Phys.: Condens. Matter 13 177

(http://iopscience.iop.org/0953-8984/13/1/318)

INSTITUTE OF PHYSICS PUBLISHING JOURNAL OF PHYSICS: CONDENSED MATTER

J. Phys.: Condens. Matter **13** (2001) 177–187 www.iop.org/Journals/cm PII: S0953-8984(01)16352-6

Helium–dislocation interaction in aluminium

Amarjeet Singh, Sanjib Maji and P M G Nambissan[1]

Atomic and Nuclear Physics Division, Saha Institute of Nuclear Physics, 1/AF Bidhannagar, Calcutta 700 064, India

E-mail: gopal@anp.saha.ernet.in

Received 14 August 2000, in final form 24 October 2000

Abstract

Helium–dislocation interaction during the isochronal annealing of high energy He-implanted aluminium is studied using positron annihilation techniques. While helium is strongly trapped by the dislocations, the binding appears not to be strong enough to delay the annealing stages significantly. The nucleation of helium bubbles is delayed but the helium atoms do not hold the dislocations stable against annealing. The estimation of the helium bubble parameters was carried out taking into consideration the expansion of the lattice during the annealing and the bubble pressure is higher than that at room temperature, as expected. A polynomial relation is obtained between the helium melting temperature and the helium atom density. The bubbles are highly overpressurized and could serve as ideal systems for exploring the Simon–Glatzel transition expected at low temperatures.

1. Introduction

Despite the many review articles and papers published during the last few years on the subject of helium bubble formation and growth in metals and alloys [1–5], proper attention seems to be still needed on the influence of dislocations on the said processes. During high energy implantation of energetic alpha particles in solids, a small density of dislocations is generally produced along with other point defects and defect clusters. The extent to which the dislocations can trap helium needs to be investigated, at least to delineate their role from that of the better explored species of defects such as vacancies and vacancy clusters.

Among the numerous versatile experimental probes available for investigation, positron annihilation stands unique as a viable spectroscopic method to study the defects and defect–impurity interactions over a wide range of types, size and concentration. In many metals, the positron lifetimes in monovacancies and point dislocations are rather close such that the instrumental resolution fails to indicate their respective interaction with light gas ions seperately. This has made it difficult to comment on the interaction of dislocations with helium or other inert gas ions from studies where the evolution of vacancies or their clusters into dense bubbles obtained better coverage. This paper attempts to highlight how the dislocations present

[1] Author for correspondence.

0953-8984/01/010177+11$30.00

in a metal prior to helium implantation can affect the initial stages of bubble formation and growth by carrying out a unique experiment described below and focuses on a few important aspects of helium bubble parameters derived from the existing positron surface state model [6] and the high density equation of state [7].

2. Experiment

High purity (6 N) aluminium single crystalline samples were annealed in high vacuum for several hours at 900 K to obtain a perfect defect-free state. Two pairs of samples were prepared: one with a thickness of 1 mm, the other—with an initial thickness of 3 mm—was deformed to 65% reduction in thickness to saturate it with a high density of dislocations. Helium atoms of energy varying from 3 MeV to 45 MeV in regular discrete steps were implanted in both the pairs of samples to a total dose of 10^{18} cm^{-2}. This gave a net input helium concentration of about 300 p.p.m. A ^{22}Na source was sandwiched between the pairs of samples for positron annihilation experiments. Positron lifetime measurements were carried out using a slow–fast coincidence set-up with 240 ps resolution (fwhm) for ^{60}Co prompt gamma rays. The data were analysed using RESOLUTION and POSITRONFIT [8]. Doppler broadening measurements were also carried out using a 40 cm^3 HPGe detector having a resolution (fwhm) 1.14 keV at 514 keV (^{85}Sr). The conventional S parameter was used to interpret the data [9].

The samples were isochronally annealed at intervals of 25 K from 300 to 900 K for 1 hour at each temperature and in high vacuum (10^{-3} Pa) followed by slow cooling in vacuum to room temperature. Measurements at room temperature were carried out after each annealing.

3. Results and discussion

The analysis of the S versus T variation shown in figure 1 indicated evidence to suggest strong interaction between the helium atoms and the existing matrix of dislocations in the initial stages of isochronal annealing. As is expected, the helium atoms are mobile in aluminium at moderate temperatures and are likely to be trapped in vacancies and other types of heterogeneity such as dislocations and grain boundaries. The behaviour of the two curves at higher temperatures is similar, showing the stages of helium–vacancy interaction, formation and growth of larger helium bubbles and further growth aided by thermal vacancy condensation.

In the discussion on the results of the positron lifetime experiments, only the longer lifetime component τ_2 and its intensity I_2 are considered, for the shorter lifetime τ_1 invariably reflected consistency with the two-state trapping model normally prevalent in such situations [10]. This model assumes that the positron annihilates either in the bulk of the metal with a rate λ_b or after getting trapped in the defect, in which case the annihilation rate is reduced to λ_d. The kinetic equations governing the decay of the number of positrons in the respective states then will have the form

$$\frac{\mathrm{d}n_b}{\mathrm{d}t} = -\lambda_b n_b - \kappa n_b \tag{1a}$$

and

$$\frac{\mathrm{d}n_d}{\mathrm{d}t} = -\lambda_d n_d + \kappa n_b \tag{1b}$$

where κ is the rate of trapping of positrons from the bulk to the defects. Assuming that initially all the positrons are released into the bulk, i.e $n_b(t = 0) = 1$ and $n_d(t = 0) = 0$, the above

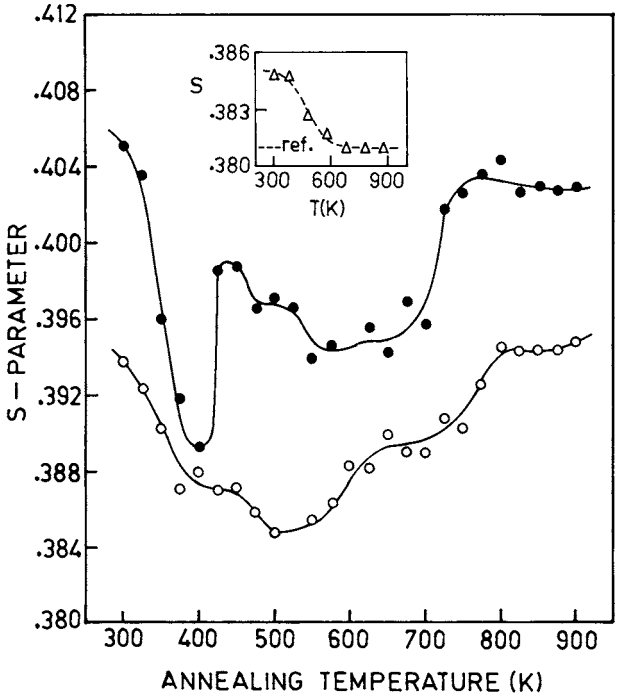

Figure 1. The S parameter versus annealing temperature variation for the helium-implanted Al samples; open circles denote the data for the non-deformed sample and the closed circles those of the deformed one. The inset shows the corresponding variation for a plastically deformed but unimplanted Al sample.

two equations can be solved to get

$$n(t) = n_b(t) + n_d(t)$$
$$= \frac{\lambda_b - \lambda_d}{\lambda_b - \lambda_d + \kappa} \exp[-(\lambda_b + \kappa)t] + \frac{\kappa}{\lambda_b - \lambda_d + \kappa} \exp(-\lambda_d t). \tag{2}$$

After deconvoluting the instrumental resolution function and correcting for the effects of source and background, each of the experimental positron lifetime spectra could be decomposed into two components such that

$$n(t) = I_1 \exp(-t/\tau_1) + I_2 \exp(-t/\tau_2). \tag{3}$$

A comparison of the equations (2) and (3) gives a direct relation for the estimation of the positron lifetime ($\tau_b = \lambda_b^{-1}$) in the bulk of the metal in terms of the measured lifetimes τ_1, τ_2 and their intensities I_1 and I_2. The lifetime thus estimated

$$\tau_b^{cal} = \left(\frac{1}{\tau_1} - \kappa\right)^{-1} \tag{4a}$$

with

$$\kappa = I_2 \left(\frac{1}{\tau_1} - \frac{1}{\tau_2}\right) \tag{4b}$$

should be independent of the individual variations of τ_1, τ_2, I_1 and I_2. As illustrated in figure 2, the interpretation of the present results in terms of the two-state trapping model in both the

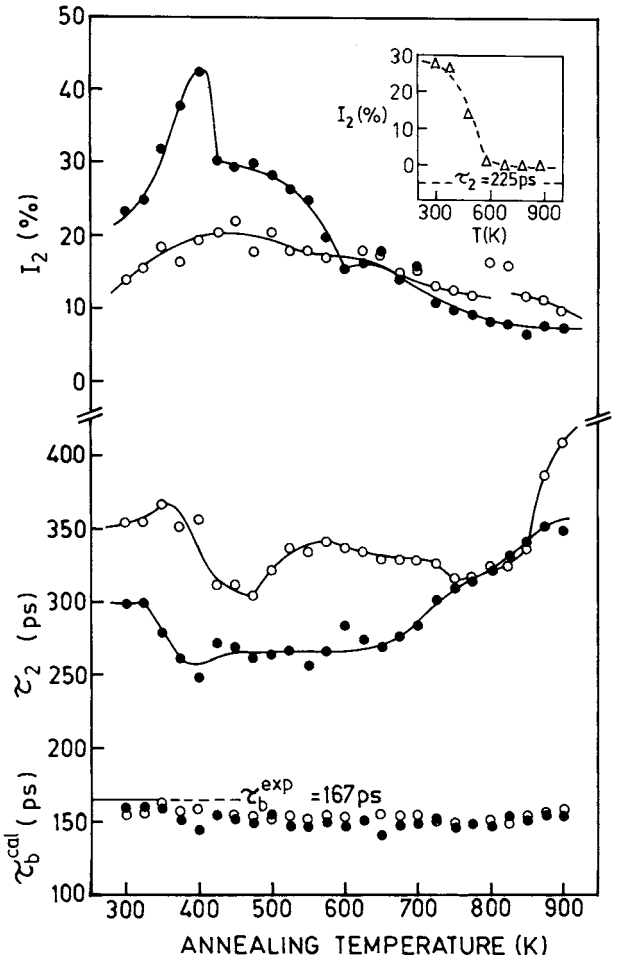

Figure 2. The variation of the positron lifetime τ_2 and intensity I_2 with the annealing temperature in the helium-implanted non-deformed (open circles) and deformed (closed circles) Al samples. The inset shows the corresponding variation of I_2 (τ_2 is fixed at 225 ps, the positron lifetime in dislocations) in the case of an Al sample, plastically deformed but *not* implanted by helium ions.

samples is thus justified and the actual defect kinetics could be discussed on the basis of the changes in τ_2 and and its intensity I_2.

The longer lifetime τ_2 in fact represents the annihilation of positrons in the dominant trapping centres at the respective annealing stages, namely the helium–vacancy complexes, helium decorated dislocations and loops and bubbles. When compared with the trend of variation in the case of the reference non-deformed sample, the variation of both τ_2 and I_2 in the temperature region 300–425 K of the deformed sample is indicative of helium decoration of dislocations and loops (figure 2). The subsequent region of bubble growth, seen to commence at 475 K in the non-deformed sample, results from the migration and coalescence of small bubbles into larger ones and the bubbles then are held stable over a wide range of temperatures from 600 to 750 K. The stabilization of the bubbles probably results from the segregation of transmutation-induced Na impurities on the bubble surfaces, as discussed by Jensen and co-workers [3]. Beyond this region, further bubble growth is observed and could be attributed

to the condensation of thermal vacancies into the bubbles. In the deformed sample, these stages are seen characteristically delayed. For example, the bubble growth resulting from migration and coalescence starts after 600 K only. An independent experiment on a pure Al single crystalline sample deformed identically (but not implanted with helium atoms) showed the annealing of dislocations being complete at around 600 K (insets in figures 1 and 2). This indicates that the formation and migration of the helium bubbles are strongly impeded by the dislocations and take place only after the latter are annealed out of the sample. It may also be noted that the helium atoms decorating the dislocations are unable to hold the dislocations stable against thermal annealing. In other words, the binding of the helium atoms with the dislocations appears rather weak. Once the dislocations are fully annealed out, the released helium atoms get strongly attracted to the vacancy-type defects and their interaction result into the formation of large bubbles. As the annealing temperature has already crossed the energy necessary for the migration of small bubbles, a rapid bubble growth stage is observed from 600 K onwards.

A few comparative observations are strikingly evident. The positron lifetime in the bubbles in the as-implanted deformed samples is 50 ps less than that in the non-deformed sample. Indirectly this implies a smaller bubble size in the deformed samples. While a detailed analysis of the positron lifetime data to get quantitative inferences on the bubble properties will be discussed shortly, the smaller bubble size in the deformed samples is indicative enough to highlight the role of dislocations in restricting the free growth of bubbles. The possibility of the production of grain boundaries due to the deformation strain is also not ruled out, in which case, the grain boundaries will also have a reducing influence on void growth [11]. The intensity I_2 in the deformed sample, on the other hand, is larger compared to that in the reference non-deformed sample, implying that the dislocations do provide a favourable environment for bubble nucleation. Bubble coarsening is further indicated in both the samples by gradual reduction of I_2 at the higher annealing temperatures.

Quantitative understanding of the properties of helium bubbles nucleated in implanted materials is essential to the understanding of the bubble growth kinetics under temperatures identical to that in reactor environments. Aluminium being a metal of relatively low melting point is ideal for systematically following the sequential changes in the densities and pressures of the bubbles formed under thermal conditions. The positron surface state model, proposed by Jensen and Nieminen [6], has been in universal use for more than a decade to estimate the helium atom density n_{He} from the measured positron lifetime τ_2 (attributed to helium bubbles). This relation, when the positron lifetime is expressed in picoseconds and n_{He} in Å^{-3}, has the form

$$\tau_2 = 500 - 2350 n_{He} \tag{5}$$

where 500 ps stands for the saturation lifetime of positrons trapped at the clean metallic surface of a fully grown void in Al. As the helium atom density thus obtained is comparable to metallic densities ($\sim$0.06 Å^{-3} in Al), the effects of deviation from the ideal gas behaviour need to be considered for the estimation of the corresponding bubble pressure. Trinkaus [7] has suggested an approach in which the helium atom density obtained from equation (5) together with a compressibility factor $Z = Z(T, T_m, n_{He})$ would denote the corresponding thermodynamic variable in an otherwise ideal-like gas equation

$$P = k_B T Z n_{He} \tag{6}$$

where k_B is the Boltzmann constant. The evaluation of Z needs to examine the changes of volume associated with a given helium atom when the bubble is expected to melt at the temperature T_m. In other words, one can equate the fluid volume per atom upon freezing v_l given by Trinkaus [7] as

$$v_l = 56 T_m^{-1/4} \exp(-0.145 T_m^{+1/4}) \qquad \text{in } \text{Å}^3 \tag{7}$$

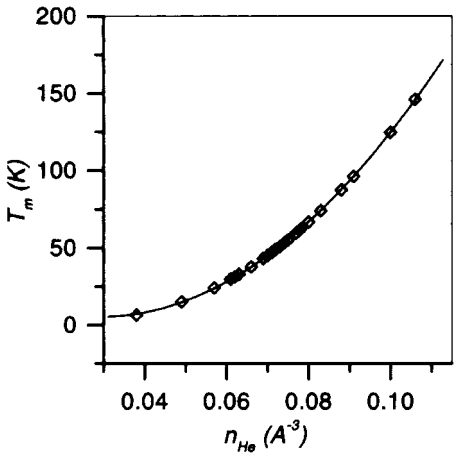

Figure 3. The polynomial relation (solid line) between the melting temperature of helium and the density of helium atoms.

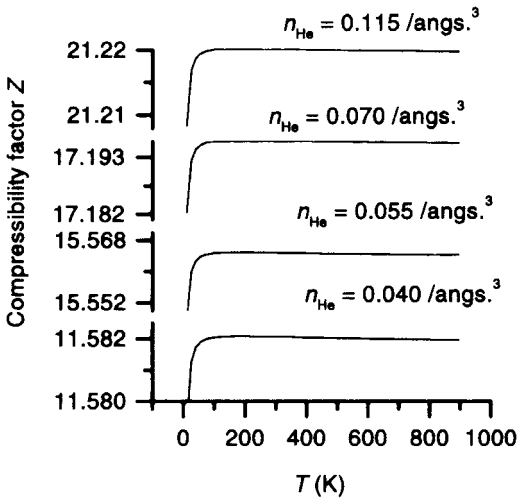

Figure 4. The variation of the compressibility factor Z with temperature for four different helium atom densities.

with the sum of the solid volume per atom $v = 1/n_{He}$ and the change in that volume due to melting as can be obtained from the Clausius–Clapeyron equation. Mills *et al* [12] had empirically related the change in molar volume of helium upon melting with the melting pressure P_m by the relation

$$\Delta V_m = 0.6640(P_m + 1.604)^{-0.3569} \tag{8}$$

so that the fluid volume v_l can be written as

$$v_l = v + \Delta V_m / N_A \tag{9}$$

where N_A is the Avogadro number. Solving the equations (7) and (9) with the help of the Simon-type equation [12]

$$P_m(\text{GPa}) = 0.001\,691 T_m^{1.555} - 0.000\,8112 \tag{10}$$

the melting temperature T_m was obtained for the different values of n_{He} and plotted in figure 3. It is significant to observe a systematic variation of the melting temperature with the density of helium atoms (in Å^{-3}) in the bubble and the two variables can be fitted with a polynomial (solid line in the figure) as given below.

$$T_m(\text{K}) = 25.083 - 1.374 \times 10^3 n_{He} + 2.369 \times 10^4 n_{He}^2. \tag{11}$$

The compressibility factor Z in the final form is given by the expression

$$Z = (1-\rho)(1+\rho-2\rho^2) + (1-\rho)^2 B(T) n_{He} + (3-2\rho)\rho^2 z_l - 50(1-\rho)\rho^2 \tag{12}$$

where the virial coefficient $B(T) = 170T^{-1/3} - 1750T^{-1}$ (in Å^3) and the compressibility on freezing $z_l = 0.1225 v_l T_m^{0.555}$. The reduced particle density ρ is defined as $\rho = v_l n_{He}$ and equation (12) has been successfully used as an appropriate equation of state for high density helium bubbles in a number of recent studies [13–15].

Certain basic features of the dependence of the compressibility factor Z on the temperature of bubble formation and helium atom density in the bubbles are revealed in figures 4 and 5. It can be noted from figure 4 that the dependence of Z on temperature is rather indirect and the actual need to modify the ideal gas equation in fact originates from the strong helium–helium

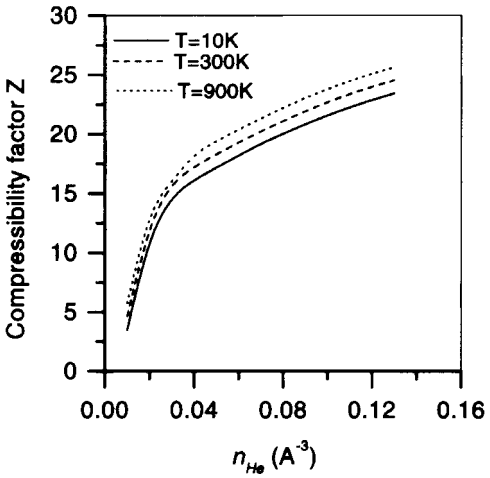

Figure 5. The Z versus n_{He} variation at three different temperatures. The lines in fact overlapped but are vertically shifted for clarity.

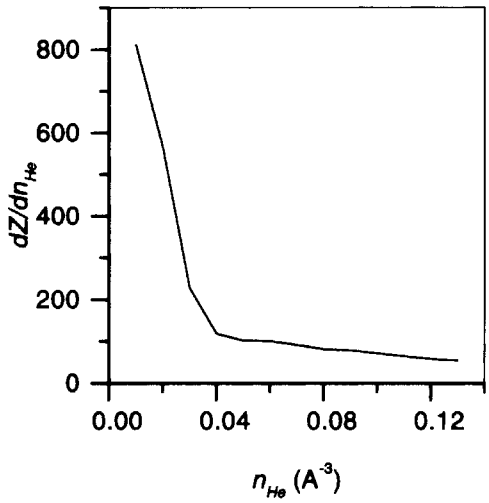

Figure 6. The variation of $\mathrm{d}Z/\mathrm{d}n_{He}$ with n_{He}.

interaction as may be expected from the high helium atom density discussed earlier. The dependence of Z on n_{He} over the complete range of helium atom densities dealt with in the present experiment is illustrated by the three isotherms in figure 5. Initially at lower values of n_{He}, the variation of Z is very sharp and can be understood as due to the 'softness' of the atoms, which permits them to be at closer proximity than in an ideal gas where the atoms are conceived as rigid spheres. The compressibility however may attain saturation at very high densities, an indication of which is evident from the $(\mathrm{d}Z/\mathrm{d}n_{He})_T$ versus n_{He} curve shown in figure 6.

In non-equilibrium experiments where the positron lifetimes are normally measured at room temperature after cooling the samples following the corresponding heat-treatments, the use of the temperature T and the helium atom density n_{He} in equation (6) needs to be consistent with the actual experimental situation. This means when the helium bubble pressure P is calculated from the measured n_{He} and the room temperature in equation (6), the interpretation of the results can be unrealistic for want of consideration of the explicit dependence of the bubble pressure on the temperature and of the thermal expansion of the host metal on the helium atom density during the annealing. In order to verify this conjecture, the bubble pressure corresponding to each annealing temperature was estimated in two ways, one (P_{RT}) using room temperature and the helium atom density obtained from equation (5) and the other (P_T) using the annealing temperature and the helium atom density appropriately scaled to consider the effects of lattice expansion of aluminium due to the change from the room temperature to the annealing temperature. For the scaling, we first estimated the helium bubble radius at room temperature after each annealing from the quadratic equation [13–15]

$$\frac{H}{A}r_B^2 + \frac{H}{B}r_B - 1 = 0 \tag{13}$$

where $H = (4\pi n_{He}\kappa_B)/(3S_f N_{He})$. The total input helium concentration N_{He} is calculated from the initial implanted helium dose and energies and the positron trapping rate κ_B is obtained from the measured positron lifetimes and intensities using equation (4*b*). The scaling factor S_f is used to account for the dependence of the trapping efficiency on n_{He} as discussed by Jensen and Nieminen [6]. $A = 9.07 \times 10^{15}$ Å^{-1} s^{-1} and $B = 3.30 \times 10^{14}$ Å^{-2} s^{-1} are

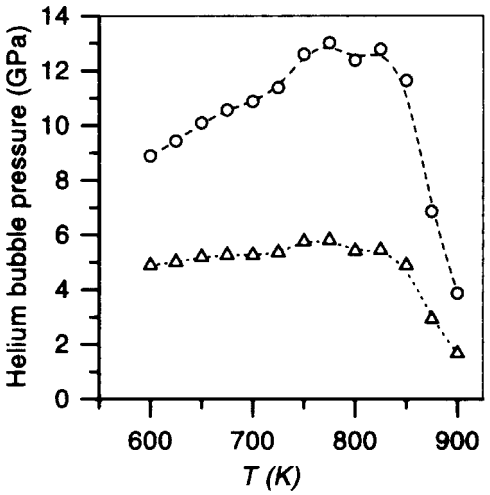

Figure 7. Variation of helium bubble pressures P_T (○) and P_{RT} (△) with annealing temperature above 600 K in the non-deformed sample.

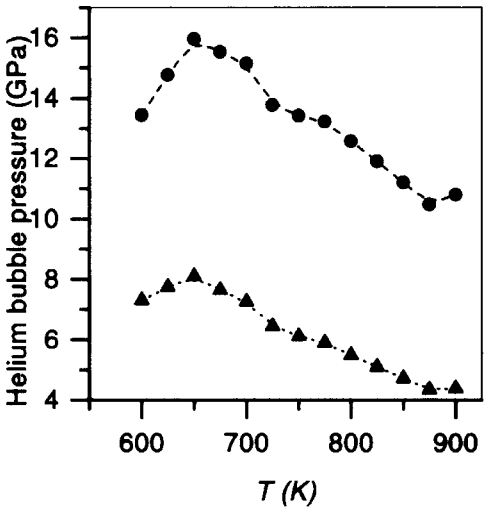

Figure 8. Variation of helium bubble pressures P_T (●) and P_{RT} (▲) with annealing temperature above 600 K in the deformed sample.

empirical constants. Assuming realistically that all the input helium is contained in the bubbles and further that the bubbles are spherical in shape with the mean radius r_B, an equation of consistency can be framed as

$$N_{He} = \tfrac{4}{3}\pi r_B^3 C_B n_{He}. \tag{14}$$

We assume that the helium bubble concentration C_B during the cooling of the sample does not change owing to decreasing thermal energy otherwise available for the bubbles to migrate and the only possible effect is the lattice contraction of the host metal. In such a case, the actual bubble radius at the culmination of the annealing at a particular temperature T can be estimated as $r_B^T = r_B(1 + \alpha T)$ with the linear thermal expansion coefficient of Al considered to be proportional to T above the Debye temperature ($\theta_D = 394$ K). Since helium is unlikely to escape from the samples, we can equate to the same N_{He} in equation (14) the re-estimated helium concentration in terms of r_B^T and obtain the helium atom density n_{He}^T at the particular annealing temperature. The pressure (P_T) thus estimated using the corresponding T and n_{He}^T is shown against the annealing temperature of the reference non-deformed sample in figure 7. For comparison, the pressure (P_{RT}) calculated using room temperature and n_{He} obtained from equation (5) is also shown. The corresponding results for the deformed sample are shown in figure 8.

There are certain interesting implications of these results, as will be discussed in the following. In both the cases, $P_T > P_{RT}$ despite the helium atom density being smaller during the annealing than after cooling to room temperature. (For clarity, we have illustrated three representative cooling characteristic curves for the bubble pressure in figure 9.) The higher bubble pressure during the annealing would imply the likelihood of occurrence of favourable pressure relaxation processes, such as dislocation loop punching. While the variation of P_{RT} with annealing temperature in the temperature range 600 to 800 K of the non-deformed sample does not indicate any pressure build-up that could lead to the subsequent relaxation above 800 K, it is amply indicated by the rise of P_T in this range. Even though the role of thermal vacancy condensation is reflected in the sharp fall in pressure, P_T appears to be a more sensitive parameter compared to the normally adopted P_{RT}. Identical arguments equally hold good in the case of the deformed sample as well. There are however striking differences

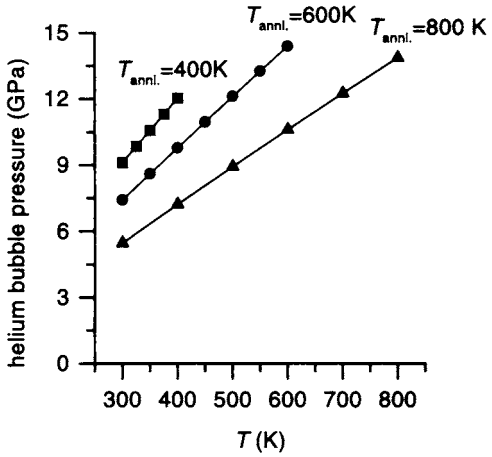

Figure 9. The drop in helium bubble pressure while cooling the sample to room temperature after annealing at three different temperatures.

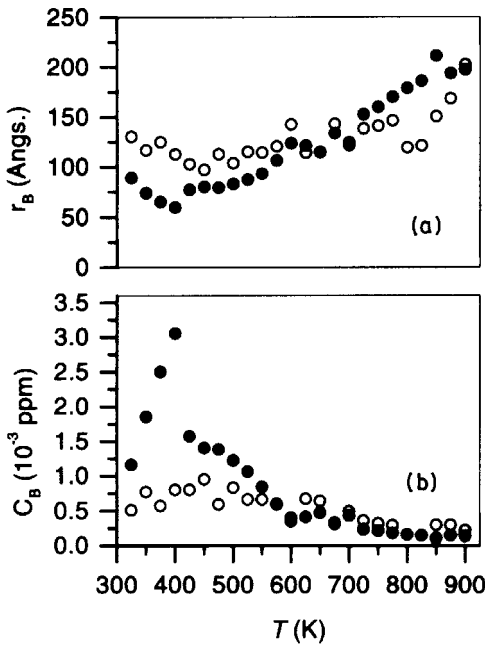

Figure 10. The variation of (a) the bubble radius r_B and (b) bubble concentration C_B with annealing temperature in the two samples (open circles denote the non-deformed sample and the closed circles denote the deformed sample).

which are worth special mention, like the observation of relatively higher bubble pressure in the deformed sample. The dislocations (and perhaps grain boundaries too) which had been initially present in the deformed sample had severely restricted the growth of bubbles. Another justification for this statement may be seen in figure 10 where the mean bubble radius in the deformed sample is smaller than that in the non-deformed sample, in contrast to the bubble concentration. Both are indicative of the accommodation of a larger number of helium atoms

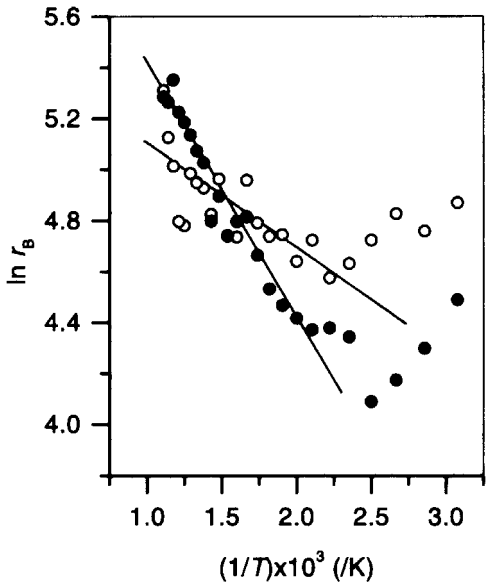

Figure 11. The Arrhenius plots depicting ln r_B against the inverse ($\times 1000$) of the annealing temperature.

in the bubbles in the defomed sample. Although at higher annealing temperatures the bubble radius in the deformed sample appears to be larger than in the non-deformed one, the pressure in the former remains larger than that in the latter. This is a strong indication of the role of dislocations in favouring the formation of higher density bubbles of smaller dimensions even while they are annealed out without being stabilized by the helium atoms.

A further verification of the above argument may be presented with the help of figure 11, where the Arrhenius plots depicting the variation of the bubble radius versus the scaled inverse of temperature ($1000/T$) have been shown. Since the data points are highly scattered, we have adopted the following method to draw the solid lines in the figure. For each sample, any two points towards either extremes (corresponding to the temperature range 600–900 K only) were selected at random and the slope is determined. Taking the average of the slopes obtained from several such combinations, the line was drawn and an activation energy of 0.04 eV has been obtained in the non-deformed sample. In the deformed one, the corresponding value thus obtained was approximately 0.08 eV. Notwithstanding the crudeness of the model being used to estimate the bubble radius, the two activation energies differ by a factor of 2, suggesting that bubbles with higher densities certainly are likely to suffer from less mobility and their migration accordingly may be partly impeded.

In all the cases discussed above, the bubble pressure is much higher than the equilibrium bubble pressure given by $P_{eq} = 2\gamma/r_B$ where γ is the surface tension of Al ($\sim$1 N m^{-1}). The bubbles are thus extremely overpressurized and will be driven to partial relaxation of the pressure under suitable conditions such as the generation of thermal vacancies. The actual bubble pressures at certain temperatures are as high as 5–6 GPa. The Simon–Glatzel relation connecting the freezing temperature T_m of helium with the corresponding bubble pressure P_m is given by

$$P_m(\text{GPa}) = A[(T_m/T_0)^c - 1] \tag{15}$$

with $A = 0.0051$ GPa and $c = 1.5602$ constants and $T_0 = 2.045$ K for He. For $P_m = 6$ GPa,

the equation predicts a freezing temperature for helium as high as ∼190 K and is a temperature attainable in standard cryogenerators. Experiments to investigate such a transition have been carried out recently and the results will be soon published elsewhere [16].

4. Conclusions

It is demonstrated in this study that a systematic and quantitative investigation of the interaction of helium with dislocations is possible by implanting helium atoms directly into a dense matrix of dislocations. The effects of helium–vacancy interaction thus can be fully delineated. We see that dislocations can act as very strong trapping centres for helium deposition and the clustering process (in other words, the formation of bubbles) at the dislocation sites is a more intensified one, resulting in denser bubbles compared to those in a non-deformed helium-implanted sample. Quantitative analysis using the positron surface state model and the high density equation of state points towards the formation of highly overpressurized helium bubbles.

We further observe that the melting temperature of helium under high pressure can be polynomially fitted with the helium atom density and the relation makes it possible to directly estimate the former if the latter is experimentally measured either through positron annihilation or other experimental methods such as transmission electron microscopy.

It may be noted that the pressure corresponding to the actual annealing temperature estimated by scaling the helium atom density for the effects of lattice contraction is higher than the bubble pressure at the room temperature, although the helium atom density is reduced by the said scaling. This implies that temperature has the dominant role over the helium bubble dynamics than the density of atoms.

Acknowledgments

The authors wish to thank Professor Prasanta Sen for his constant encouragement throughout this work. Technical assistance from Mr Sujib Chatterjee is also gratefully acknowledged.

References

[1] See, for, example Ullmaier H (ed) 1983 *Proc. Int. Symp. on Fundamental Aspects of Helium in Metals, Radiat. Eff.* **78**
[2] Donnelly S E 1985 *Radiat. Eff.* **90** 1
[3] Jensen K O, Eldrup M, Singh B N and Victoria M 1988 *J. Phys. F: Met. Phys.* **18** 1069
[4] See, Donnelly S E and Evans J H (eds) 1991 *Fundamental Aspects of Inert Gases in Solids* (New York: Plenum)
[5] Eldrup M 1992 *Mater. Sci. Forum* **105–110** 229
[6] Jensen K O and Nieminen R M 1987 *Phys. Rev.* B **35** 2087
Jensen K O and Nieminen R M 1987 *Phys. Rev.* B **36** 8219
[7] Trinkaus H 1983 *Radiat. Eff.* **78** 189
[8] Kirkegaard P, Eldrup M, Mogensen O E and Pedersen N J 1981 *Comput. Phys. Commun.* **23** 307
[9] Siegel R W 1980 *Annu. Rev. Mater. Sci.* **10** 393
[10] Hautojarvi P and Corbel C 1995 *Proc. Int. School Phys. 'Enrico Fermi' Positron Spectroscopy of Solids* ed A Dupasquier and A P Mills Jr (Amsterdam: IOS Press) p 491
[11] Lane P L and Goodhew P J 1983 *Phil. Mag.* A **48** 965
[12] Mills R L, Liebenberg D H and Bronson J C 1980 *Phys. Rev.* B **21** 5137
[13] Subrahmanyam V S, Nambissan P M G and Sen P 1994 *Solid State Commun.* **89** 523
[14] Subrahmanyam V S, Nambissan P M G and Sen P 1994 *Radiat. Eff. Defects Solids* **132** 169
[15] Subrahmanyam V S, Nambissan P M G and Sen P 1996 *J. Phys. Chem. Solids* **57** 319
[16] Maji S, Singh A and Nambissan P M G 2000 *Phys. Lett.* A submitted